TENACIOUS: A Tomographic ENA Comprehensive Ion and Optical University Satellite

R. B. Sheldon

The University of Alabama in Huntsville

T. E. Fritz and H. E. Spence

Boston University Center for Space Physics

Abstract

The proposed TENACIOUS mission will provide new knowledge of the inner magnetospheric energetic particle populations through both *in situ* and remote sensing techniques. The mission payload consists of energetic neutral atom imagers, energetic charged particle, and optical sensors that will image the Earth's geocorona and inner magnetospheric neutral particle populations while also providing *in situ* measurements of energetic charged particles. TENACIOUS is optimized to measure local and remote particle populations from low-Earth orbit. The TENACIOUS mission provides a significantly different and critically important vantage point than its high-altitude counterparts. These unique data will allow us to obtain entirely new tomographic views of magnetic substorms and storms, to image the flux tubes of the auroral acceleration region, and to explore the low-altitude extension of the ring current and plasma sheet, which can be imaged easily with high temporal and spatial resolution.

Introduction: The Significance of and Scientific Basis for Magnetospheric Imaging

Great progress has been made recently in magnetospheric imaging. Beautiful images of energetic neutral atoms (ENAs) created by ion collisions with the Earth's tenuous upper atmosphere have been collected by several satellites, including NASA's POLAR satellite. These new global images demonstrate the feasibility and scientific usefulness of remote sensing to understand quantitatively the magnetospheric response to solar events [*Jorgensen et al.*(1997), *Henderson et al.*(1997),]. In the Tomographic Energetic Neutral Atom Comprehensive Imaging University Satellite (TENACIOUS) mission, we propose a suite of instruments that will substantially increase our knowledge and insight into the magnetospheric responses by providing *in situ* measurements of particle fluxes and supporting optical emissions to complement ENA imaging. Ultimately, with this new knowledge, we will be able to better understand and predict the magnetic substorms and storms that energize and transport energetic particles in the geospace environment.

The power of ENA measurements from spacecraft has been amply demonstrated recently on orbit (ASTRID, POLAR, GEOTAIL) - but particularly so at high altitudes by the CEPPAD/IPS on the NASA POLAR spacecraft. The TENACIOUS ENA imager we propose is based directly on the CEPPAD experiment. A schematic of how POLAR remotely senses the ENAs produced by charge exchange between the geocorona and the energetic ions of the ring current is shown in Figure 1. This figure illustrates how a two dimensional image of the optically-thin ENA emissions can be formed from a single vantage point.

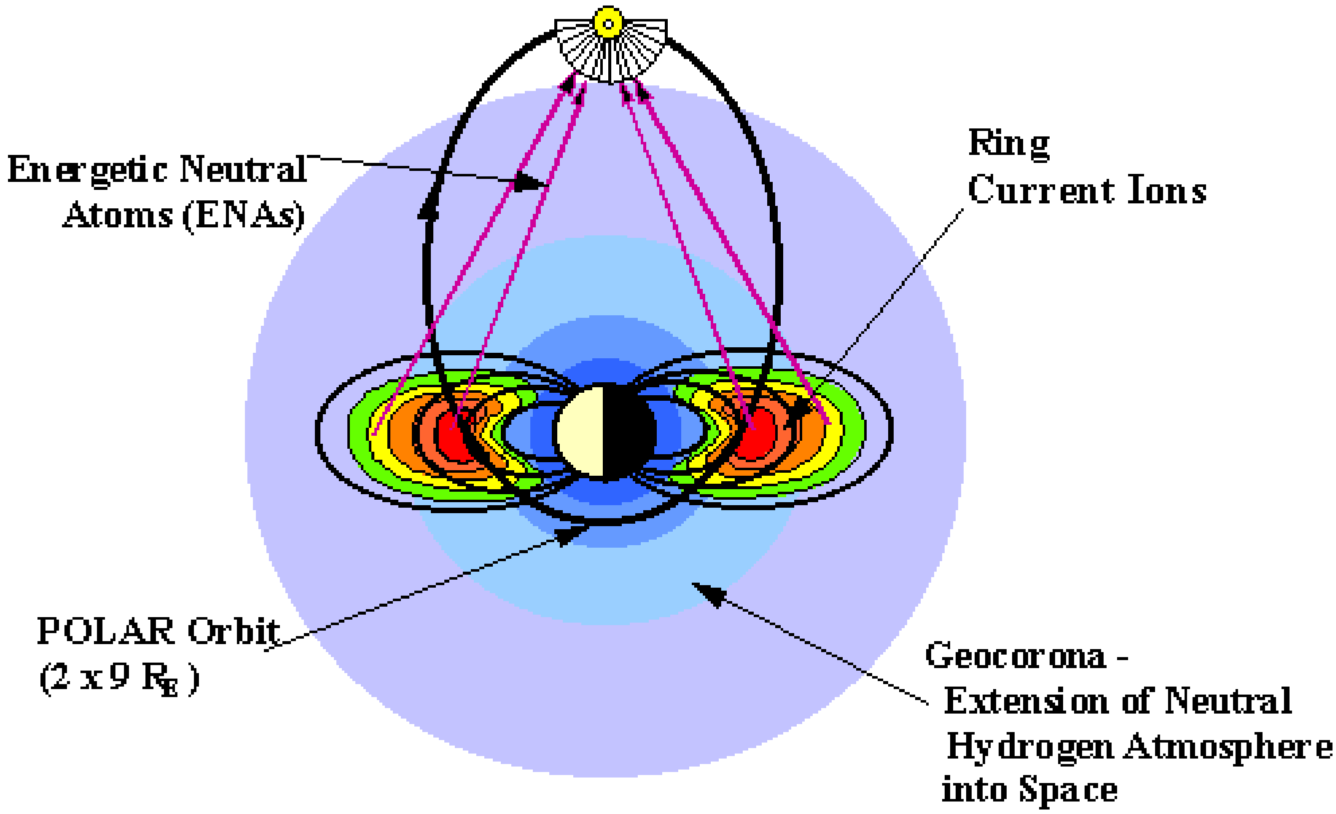

Figure 1. Schematic of Global Energetic Neutral Atom Imaging

From high apogee orbits, ENA images can be obtained on a global scale. However, ENA emissions are optically thin and involve the convolution of three-dimensional neutral and ion density distributions, interacting with an energy-dependant charge exchange cross-section. Thus, data from a single ENA sensor provides a non-unique determination of the important ion fluxes along the line-of-sight. Ideally, multiple measurements are required to obtain an unambiguous spatial distribution. With the IMAGE and TWINS missions, NASA has taken the necessary first step toward stereoscopic imaging of geospace with neutral atoms, a high scientific priority identified by NASA in their Sun-Earth Connection Roadmap and also by the NAS/CSSP. However, as [*Gruntman*(1997)] points out in his excellent review article on ENA imaging, views from both the "outside looking in" (POLAR, IMAGE, TWINS) and from the "inside looking out" (our proposed TENACIOUS mission) are critically needed in order to extract the most meaningful physical information from the images. This need is driven by the fact that the highest spatial resolution and tomography can be obtained only from low altitudes where the optically thin emissions are the brightest.

We note that dynamic magnetospheric regions connect magnetically to low-altitudes at mid- to high-magnetic latitudes. The feet of the flux tubes threading the inner magnetosphere and inner magnetotail connect to the ionosphere in regions where the geocoronal density is high. Therefore, ENA emissions are focused in these regions and the emissions are bright. A low altitude spacecraft has two important advantages over those imaging from high apogee. First, it is closer to the source region which means that the emissions will be bright and will provide higher spatial resolution images for the same angular resolution imager. Second, the spacecraft location is rapidly changing which means that the imager will provide a sequence of images of the same emission region but from lines-of-sight that are constantly changing. These two features allow for tomographic inversions to be performed with TENACIOUS, just in the same way that the BU TERRIERS STEDI mission could provide tomographic 3-D images of the upper atmosphere and ionosphere.

Overarching Scientific Goals and Objectives

Two of the most important dynamic features of the magnetosphere are geomagnetic storms, characterized by ring current intensifications with Dst variations, and substorms, characterized by magnetotail reconfigurations with auroral electrojet variations. Each event is a global magnetospheric response to changes in the solar wind and interplanetary magnetic field. For the past thirty years, we have been limited in our ability to understand the global nature of these phenomena. While we have amassed a great volume of single-point, *in situ* measurements that provide the global picture in an average, static sense (space climatology), we have lacked an instantaneous view of large-spatial-scale magnetospheric dynamics (space weather). This lack of a global perspective has limited our analysis of the *in situ* measurements. In addition, the lack of these global data limit our ability to differentiate between various physical models that describe magnetic storms and substorms. These limitations include inadequate global knowledge of particle origins, loss processes, transport mechanisms and their time dependence.

Unfortunately, ions and magnetic fields are "invisible." These quantities are dynamic and can only be measured when we fly through them with a spacecraft. Single point measurements thus cannot separate temporal from spatial variability, nor can they provide a global view. The novel approach of ENA imaging however gives us the vision we need. Recently, our team has demonstrated with the POLAR instrument on which TENACIOUS is based, that both storms and substorms have strong and repeatable ENA signatures. With the advent of global ENA imaging, we are now on the threshold of major advances in our understanding of these science topics.

The TENACIOUS mission will provide new knowledge of the inner magnetospheric energetic particle populations and their dynamics through both novel remote sensing tomography of ENAs and through *in situ* measurements. The mission payload consists of an ENA imager, energetic charged particle telescopes, and optical spectrographs that will image the Earth's geocorona and the inner magnetospheric particle populations while simultaneously providing in situ ion and electron measurements. The TENACIOUS mission, with a unique low-altitude view different from IMAGE and TWINS, will allow us to best interpret the joint TENACIOUS-IMAGE-TWINS particle images. This will allow us to image the spatial distribution and spectral and temporal evolution of ions during storms and substorms with high spatial resolution.

The TENACIOUS goals will be accomplished onboard a spinning low-Earth orbit spacecraft in a polar near-sun-synchronous orientation. From low altitudes, significant portions of the inner magnetosphere ring current regions and near-Earth plasma sheet can be viewed with ENA and optical imagers along and near the orbit track. At low altitudes, the emissions are exceptionally bright both because of proximity to the source region and to the high geocoronal densities. Closeness to the source region also permits higher spatial resolution than would be possible from high apogee satellites such as POLAR, IMAGE, or TWINS. In addition, charged particle fluxes can be sampled along the 90 minute orbit. The ENA and optical images acquired from this low-altitude vantage point complement those from high apogee orbits; it is uniquely different in that it is from the inside looking out, rather than the outside looking in. Also, since the spacecraft moves through the region rapidly, it remotely samples the same region of space from changing view paths, thus allowing for true tomography of the emission regions. We stress that a three-dimensional, time dependent picture of the near-Earth plasma is essential to the physics of storms and substorms; only at low altitudes do these regions project to volumes that can be imaged at high resolution. Together, the ENA images and the particle data, along with other expected ENA data sets (such as IMAGE or TWINS), will be used to extract globally the energetic particle populations and their dynamics.

We propose to assemble a suite of sensors optimized to observe the dynamics of energetic charged particles and their interaction with neutral particles within the earth's magnetosphere from a unique low-altitude vantage point.

These sensors and the satellite that will carry them, all have excellent and proven NASA flight heritage. They will perform the following measurements with the stated goals (also outlined in Table), at an exceptionally low cost to NASA:

- obtain high-energy-spectral resolution images of ENAs with excellent time resolution, broad spatial coverage and exceptional spatial resolution in three dimensions;
- obtain ultraviolet (UV) images of major neutral species with comparable time resolution and comparable or better spatial resolution than ENA images both for ENA inversions and to determine the response of the upper atmosphere to magnetic storms and substorms;
- obtain multiple line-of-sight views of the ENA source regions along the short-period orbit to allow for true tomographic inversions of the low-altitude extension of magnetospheric particle populations and the auroral acceleration region (especially for $L < 6.6$ Re);
- provide data bases for comparison with data from other available satellites to permit stereo ENA views of the magnetosphere
- obtain *in situ* measurement of the charged particle energy distribution in regions with UV and ENA images; our orbit permits portions of the imaged regions to be directly sampled;
- quantitatively relate high spectral/spatial/temporal resolution ENA image intensities to global particle fluxes and their dynamics, both locally and remotely driven.

Table 1. Summary of TENACIOUS Scientific Objectives

o Magnetospheric Structure and Ring Current Dynamics
- Convection boundaries, energization, and global electric fields from spectra
- Ring current growth, decay, and azimuthal asymmetries
- Radiation belt physics
o Substorms and Tail Dynamics
- Substorm-related energetic particle acceleration
- Plasma sheet thinning/expansion and Substorm onset timing and location
- Auroral zone plasma pressure gradients
o Geocoronal Physics
- Response of the geocorona to changing conditions
- Non-sphericity of source region
o Auroral Structure and Acceleration
- Imaging auroral arcs, current regions, and energetic ion in/outflow regions

Geomagnetic Substorms

During a magnetospheric substorm, magnetic energy stored in the magnetotail lobes is converted, in part, to plasmasheet flow and inner magnetosphere plasma thermal energy. This energy conversion process is rapid, happening on the time scales of minutes. It produces large disturbances in the magnetotail magnetic fields and particles over broad spatial scales, perhaps starting as a highly-localized site of acceleration and thermalization and growing in scale over a short time. Because the magnetosphere is electrodynamically coupled, the energy dissipation from this reconfiguration is global, involving virtually all regions of the tail as well as the auroral ionosphere, an essential component of a substorm. The relative timing of substorm phenomena in the deep magnetotail (>40 Re), the mid-tail plasmasheet (20-40 Re), the near-tail plasmasheet (10-20 Re), the inner edge of the plasmasheet (5-10 Re), and the auroral ionosphere provide important information about the source of particle energization during substorms and the injection of hot plasma into geostationary altitudes. Statistical studies have established the average properties of substorm injections including their strength and radial and local time extent. However, the question remains as to how representative the average substorm is in terms of dynamics and spatial extent. These questions can only be answered definitively by remotely observing the system globally and analyzing the *in situ* measurements in the context of the global evolution. TENACIOUS imagers provide immediate insight into these decade old questions.

As noted previously, the promise of ENA imaging has been made clear recently by the POLAR spacecraft. POLAR has provided the first glimpse of the substorm injection region through global ENA imaging [*Henderson et al.*(1997), *Spence et al.*(1997),]. During the substorm life-cycle, ENA emissions are observed to first brighten weakly at the inner edge of the plasma sheet during a substorm growth phase, then intensify in a localized region near pre-midnight at substorm onset, and finally spread azimuthally (primarily to earlier local times) as the substorm enters the recovery phase. Thereafter the injected ions drift westward and decay while the associated ENA emissions subside. Simultaneous measurements at geostationary orbit confirm the tail stretching and subsequent ion injection while auroral images record the auroral arc brightenings and surge evolution. Despite the relative simplicity of the POLAR ENA measurements, significant qualitative understanding of the substorm injection process has already been made. The phenomena seen in the auroral zone and magnetotail are linked by the global images and the comprehensive view of spatial and temporal evolution allows us to test various substorm hypotheses.

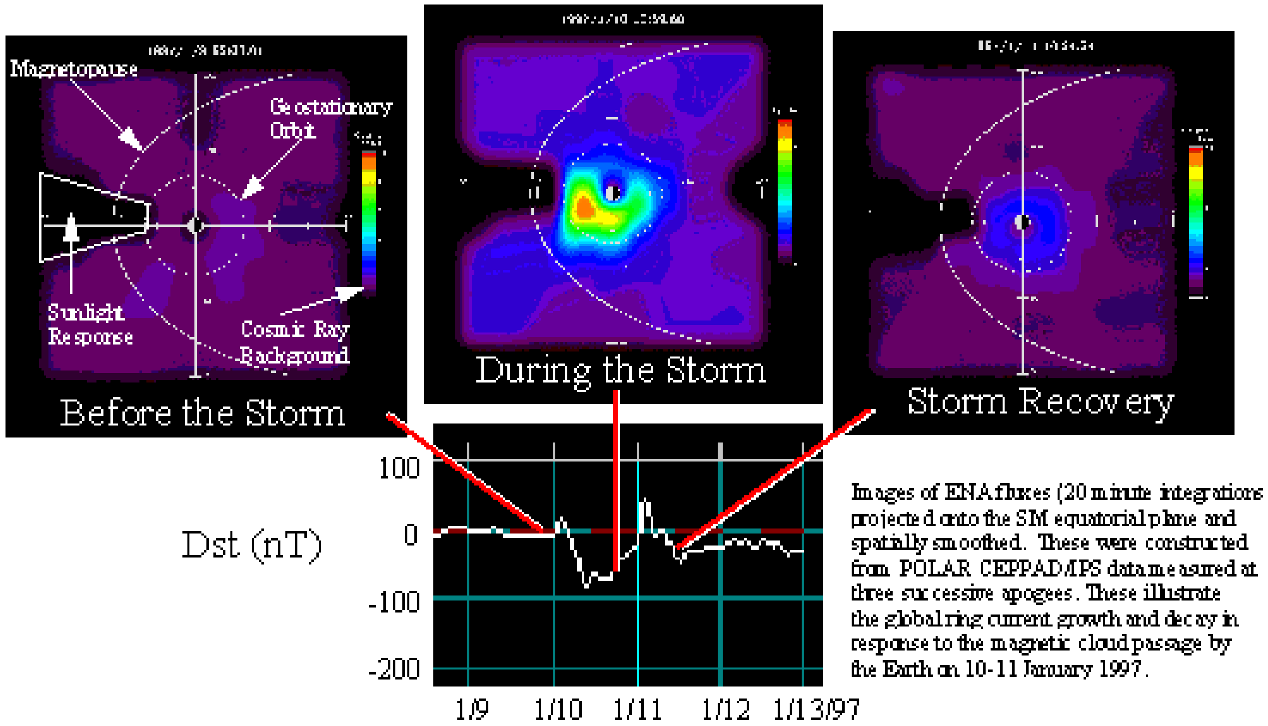

Figure 2. Global ENA Images from POLAR During a Moderate Magnetic Storm

However, these analyses are hampered by the inherent single point POLAR ENA measurements. Even with the multiple ENA data sets promised with IMAGE and TWINS, all these views are from the outside looking in and lack the ability to image with high spatial resolution the near-Earth extensions of these magnetospheric regions. For example, the middle to distant tail viewed at the magnetic equator will be virtually invisible in ENA, not primarily because there are no energetic ions, but rather owing to the very low geocoronal densities near the magnetic equator at such great distances. On the other hand, these same regions are visible from low altitudes–a small pitch-angle ion from the tail can charge-exchange in the high geocoronal densities near the Earth and thus be seen with a low-altitude ENA imager. The low-altitude, "inside-out" views provided by the TENACIOUS ENA imager will allow for substantially improved and routine observations of these regions and will complement nicely the global imaging provided by IMAGE and TWINS. Indeed, linking the high and low altitude signatures of substorms is extremely difficult with traditional methods and has led to great uncertainty in substorm model differentiation. A critical outstanding question to be answered is whether the substorm is initiated in a near-Earth current sheet disruption region that propagates tailward or is it initiated first at a near-Earth reconnection site whose effects propagate earthward? The next-generation TENACIOUS and IMAGE images should allow us to immediately establish the critical direction of propagation during a substorm and thus differentiate between competing substorm theories.

Magnetic Storms

A geomagnetic storm is characterized by the injection and energization of ions deep within the trapping region of the inner magnetosphere (L<6.6 Re). This trapped ion population decays to some resting state typically on the order of a few days. The storm time ion population is sufficiently energized such that its net guiding center drift leads to a strong enhancement of the westward-flowing, azimuthal ring current. The strong current near the magnetic equator between 2 and 6 Re depresses the Earth's surface magnetic field which defines the classic magnetic storm index, Dst. Early studies demonstrated the relationship between the energy content of the ring current and the strength of Dst as well as the large azimuthal asymmetries that can arise during the injection process (see Figure 2). Kinetic particle models rather than MHD models of the ring current are warranted owing to the large gyroradii of the pressure-bearing ions. Such models have evolved over the last twenty years but all depend on the specification of initial injected particle populations and evolving electric and magnetic fields that the particles react to during a storm cycle. These models have provided a theoretical view of the global system but until recently, have had relatively little data to constrain and test our understanding of the physics of storm injection. Most comparisons have been done with one or at most a few satellites traversing only portions of the volume important for the storm time development.

With POLAR, the growth and decay of the energetic ion population during a magnetic storm was directly tracked on a global scale for the first time using ENAs. The high geometric factor, excellent energy resolution, and capable spatial resolution of the POLAR ENA imager permit us to create global images of the ring current at high time resolution (on the order of several spacecraft spins or about one minute). An example of one such sequence of ENA images from POLAR is shown in Figure 2 during a magnetic storm in January 1997. This spatially-smoothed image shows the emissions mapped to the symmetry plane of the magnetic equator. A clear rise and fall and large local time asymmetry of the ENA flux is apparent. The partial ring current is clearly seen as fresh ions during a storm surge are injected deep into the trapping region and then drift westward owing to gradient-curvature effects; there is even evidence of ionospheric extraction of energetic ions during the main phase [*Sheldon and Spence*(1998), *Sheldon et al.*(1998),] of another storm in 1996. These ions carry an azimuthally-localized current that is seen on the ground as an asymmetric ground magnetic disturbance in local time. However, from the ground there is no clear way to know the radial or azimuthal distribution of current. Presently, only a crude asymmetry index called ASY is ever routinely produced. On the other hand, our POLAR images provide immediate global context for the analysis of point measurements within the globally imaged region. In one image, we see the local time, radial, and spectral distribution of the ring current ions and can track them in time at relatively high time resolution. These data are allowing us to test our models of electric field penetration and the complex particle accelerations during storm main phase and recovery. With TENACIOUS we will be able to obtain high spatial resolution information of the storm time ring current not possible from high apogee orbits.

Current State of Magnetospheric Imaging at High and Low Altitudes

Over the last many years, the increasing sophistication of ENA imagers has led to better empirical global views of the stormtime ring current region. Early results from the ISEE spacecraft [*Roelof et al.*(1985), *Roelof*(1987),] demonstrated the concept of quantitative use of ENA observations and ENA imaging. More recent results from the GEOTAIL spacecraft [*Lui et al.*(1996),] demonstrated the ability of ENA measurements to provide not only energy but also ring current composition. Even at low altitudes, ENA imaging studies have already amply demonstrated the power of these data, both from free-flying spacecraft, such as ASTRID measurements of the ring current [*Barabash et al.*(1997), *Brandt et al.*(1999),], and from rocket experiments, such as "Poleward Leap" measurements of auroral proton arcs [*Soraas and Aarsnes*(1996),].

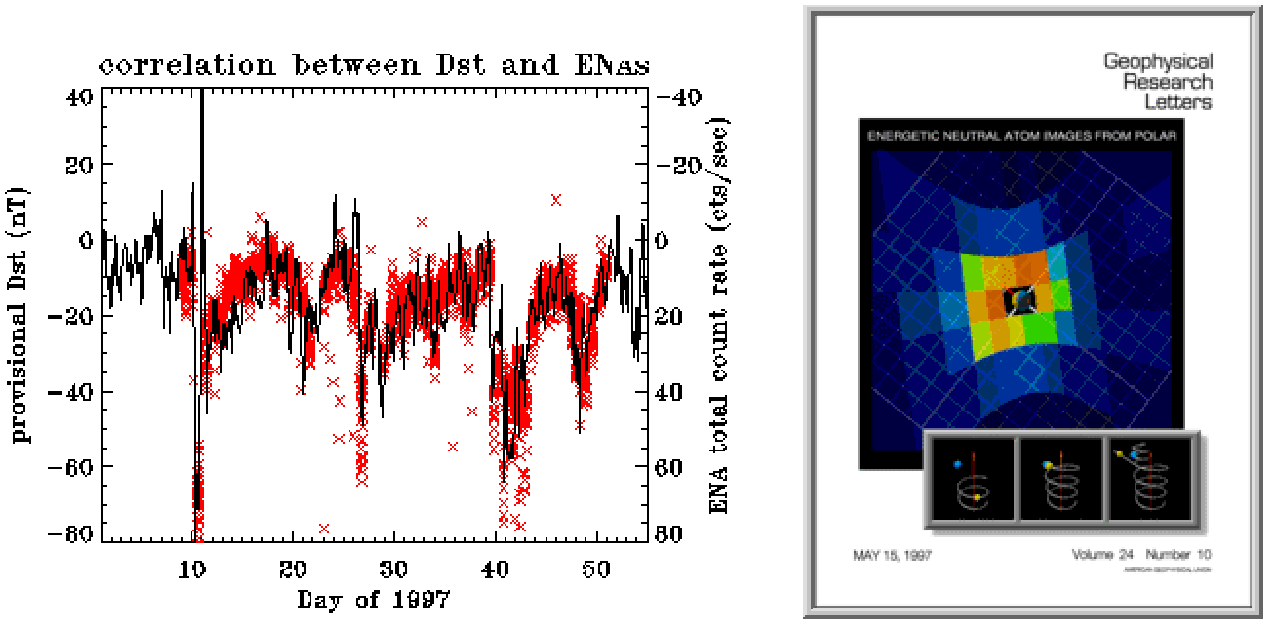

Figure 3. Correlation Between ENAs and Dst and Global Storm Imaging

The most contemporary high-altitude ENA results are from the POLAR spacecraft [*Jorgensen et al.*(1997), *Henderson et al.*(1997),] (see Figure 3) which emphasize the power of 2D imaging from a POLAR orbit and the ability to instantaneously image the entire ring current throughout a magnetic storm (see Figure 2). The POLAR ENA images permit, for example, the direct correlation of globally-integrated ENA images and the Dst index, and also are allowing us to track the stormtime injection process visually. The azimuthal asymmetry can be seen to evolve during a storm, reflecting the aggregate effects of ion drifts and the establishment and loss of the partial ring current. Despite the power of the POLAR data, the quantitative physical interpretation of the ENA images is confounded by their inherently low spatial resolution. The current pixel size projects to an area that is large in comparison to the neutral density scale height and the ion pressure gradient scale length in the ring current regions. This shortcoming represents an underconstrained data set from which it is difficult to extract unambiguous information on the populations that convolve to produce ENAs. This same problem will be encountered even by the much more capable IMAGE and TWINS imagers. By making complementary ENA images at low-altitude, the 3-D multiview and higher resolution TENACIOUS data will reduce these uncertainties and permit the important next level of quantitative analysis of stormtime injection both near the equator and possibly off the equator via parallel potentials.

For the TENACIOUS mission, we shall be observing ENAs produced within geospace but from low-altitudes, a complementary vantage point to that of POLAR (the same as IMAGE and TWINS will provide). Do we have evidence that ENAs from these low-altitude regions will actually be observed? We have every expectation they should be. The equatorial distributions have fluxes near the loss cones–often comparable to the trapped fluxes–that will mirror at lower altitudes. These lower altitudes have much higher neutral densities, often by many orders of magnitude, so the commensurate rate of ENA production could be much higher. Furthermore, a low altitude spacecraft is considerably closer to this low-altitude source region so the emitted flux of ENAs should appear brighter. Such considerations have already been treated theoretically by several studies [*Orsini et al.*(1994), *Milillo et al.*(1996), *Roelof*(1997b), *Roelof*(1997a),] and these have shown that low-altitude imaging is not only viable but is highly desirable. Indeed, as noted above, both ASTRID and Poleward Leap observations demonstrate not only the existence of low-altitude ENAs but also their high intensity and also their scientific utility. Those are reviewed below. In addition, we present exciting new evidence from the long-running TIROS mission of considerable ENA fluxes detected at low altitude and their association with storms and substorms.

[*Barabash et al.*(1997)] used the ASTRID data to show a correlation, as in Figure 3, of the ENA flux measured from a low altitude orbit (1000 km) with Dst. Their instrument had a geometric factor of 2.5 x10^{-3} cm^2-sr (somewhat smaller than that of the POLAR CEPPAD imager). Within the energy range of 26-37 keV, they observed ENA rates of 100 counts/second even during intervals of very weak ring activation (Dst $>$ -40 nT). These data were used to create maps of the ring current ions and used to do quantitative modeling of a small magnetic storm (Dst $\sim$ -80 nT) on 8 February 1995. Simulation results [*Brandt et al.*(1999),] and forward modeling revealed that during the main phase the ENAs seen at low altitude were consistent with a strong duskside source near the equator between L=4 to 8 centered at 19 MLT with a spread of about one hour of MLT. This is similar to the strong partial ring current peak observed in ENAs near the equator by POLAR.

[*Soraas and Aarsnes*(1996)] have used ENAs measured from the Poleward Leap sounding rocket to probe the structure of proton arcs in the auroral zone. They used a solid state detecting system with a geometrical factor of 4.3 x 10^{-2} cm^2-sr but were constrained to measure from altitudes below 454 km, in regions of multiple scattering in the higher density low altitudes atmosphere. At energies of 20-50 keV, they observe highly directional ENAs coming from a proton arc with rates approaching 1000 counts/second. Using these data, the study was able to observe ENAs in an arc during the expansion phase of a substorm and provide a regional map of the proton precipitation with excellent energy spectral resolution. The study showed a remarkably good agreement between the observed ENA emissions compared to a simple model of proton precipitation, even in this lower altitude regime where multiple scattering can have a blurring effect.

We note also in a study presently underway at Boston University [*Alothman and Fritz*(1998),], the discovery that even the NOAA TIROS spacecraft have been observing ENAs routinely from their 850 km polar orbit for decades. The TIROS orbit is at an altitude just midway between the rocket ENA measurements ($<$450 km) and the ASTRID measurements (1000 km). Like the Poleward Leap instrument, the TIROS energetic particle experiment is a simple solid state detecting system. However it possesses a higher energy threshold than we will fly on TENACIOUS; therefore the rates that it measures should be a lower limit approximation to what we should expect. TIROS measures ENAs at many hundred counts per second while in the polar caps looking back toward the auroral zone and ring current. Figure 4 shows a plot of TIROS ENAs, similar to Figure 3, demonstrating the relationship of ENA count rate to AL and Dst during a substorm and a magnetic storm.

In Figure 4, the solid colored crosses denote the average ENA rates measured by the TIROS spacecraft while in the polar caps looking back at the auroral zone and ring current regions. We can infer that these are ENAs by virtue of another detector looking toward the nadir which observed no discernible ion signal in the polar caps (squares).

Over the course of several day periods, during the course of two magnetic storms in 1980, we can see that the ENA rate tracks both the Dst (black heavy line) and the AL indices (green line). Indeed, it is arguable that the ENA rates track the AL curve more closely than the Dst curve, suggesting that these are ENAs associated with higher latitude, auroral phenomenon, rather than lower latitude ring current phenomenon. From these powerful data, we therefore have every confidence that the unique TENACIOUS perspective from low altitudes, with high spectral-, temporal-, and spatial-resolution ENA images coupled with optical data, will provide critical new information on both storm and substorm studies.

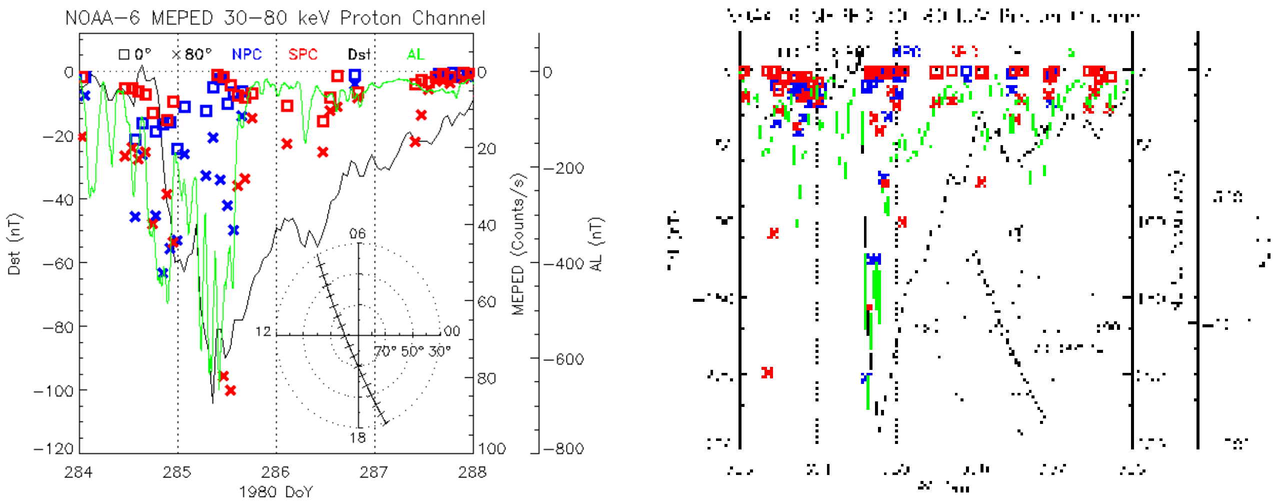

Figure 4. Correlation Between ENAs and Dst/AL From TIROS

New Applications of Low-Altitude Imaging

Auroral Acceleration

The NASA Small Explorer, FAST, has shown that the auroral zone is a region of complexity with interesting microphysics coupling to macroscale phenomenon. Part of the auroral puzzle is the distribution in space and time of auroral arcs. While FAST can make very rapid measurements, it is still limited in its ability to unravel spatial versus temporal variations. While the bulk of auroral energies are below our instrument threshold, there does exist a finite component in our energy range ($>$ 15 keV) that we are confident we can image. The TIROS and POLAR data indicate strongly that we will. Therefore, TENACIOUS has the chance of revealing the structures associated with proton aurora on a macroscopic scale. Owing to the spacecraft motion, we will then fly through the structure, possibly coincidentally, and thus be able to make excellent progress in unfolding the surrounding ion fluxes for the first time, with tomographic inversion techniques. As FAST has revealed, TENACIOUS will have the exciting possibility to image as a function of neutral atom energy two major auroral acceleration regions to complement classical optical images: the upward-accelerated ions associated with traditional auroral arc regions (from which auroral arc electric field structure may be inferred in 3D; and the so-called “black aurora” regions characterized by downward-going hot magnetospheric ions that neutralize at the feet of auroral field lines.

Radiation Belt

The mechanisms that form and accelerate the radiation belt particles can be different from the ring current. For example, both the CRAND source and the March 1991 solar wind shock produce radiation belt enhancements in a far different manner than the radial diffusion and adiabatic energization that forms the quiet time ring current. If the radiation belt ions are adiabatically transported to their low-L, high-B location, then one can confidently predict that the "source region" for the radiation belts has lower energy ions that are reduced by the ratio of magnetic field strengths, B_{source}/B_{belt}. Several regions have been proposed as sources of these ions, including the tail, the cusp and the boundary layer/ magnetosheath. None of these regions have high enough geocoronal densities to produce much ENA flux, but if they are mapped into the loss cone at low altitudes, a substantial ENA flux would result. The low altitude orbit of TENACIOUS, then, is the only place where these putative source populations could be remotely sensed. Therefore it is of great interest to spectrally resolve ENA's arising from high latitudes and differing MLT, for then we may be able to map the precursors to a radiation belt enhancement and resolve their sources.

Geocoronal Science

As powerful as the ENA measurements are, they do not return the source ion distributions without deconvolving the densities of the neutral, electron-donor background gas. On this basis alone, a measurement of the geocoronal density is essential, including not only [H], but also [He] and [O] at low altitudes. We accomplish this task by using spectroscopic tomographic inversion methods pioneered by TERRIERS, and applied to the EUV sunlight scattered by these species described later in Section D.2a. In addition to these neutral gases which form a purely gravitationally bound atmosphere, both He^{+} and O^{+} are conceivably important electron donors for ENAs whose densities would track the magnetically confined plasmasphere. [*Sheldon and Hamilton*(1993)] has shown that He and He^{+} electron donor cross sections may actually dominate over H for select species and energy of ENAs. TENACIOUS will have the ability to track photometrically the three most abundant neutral gases [H], [He], and [O], as well as the most important plasma species [O^{+}] (excluding [H^{+}] which is photometrically invisible). These geocoronal measurements will complement those being made from high altitudes with advantages similar to those described for the ENA measurements.

Finally, the geocorona is an extension of the upper atmosphere that causes satellite drag, which has high variability both annually and during the solar cycle. It should be noted that the scale height of the geocorona varies most rapidly at low altitude precisely where TENACIOUS will have the best resolution. Thus, TENACIOUS is uniquely suited to providing a 3-D, time variable, dynamic geocoronal model.

Complementarity to Other NASA Neutral Atom Imaging Missions

As noted above, TENACIOUS is complementary with other planned NASA ENA imaging missions and should not be perceived as merely duplicating other related measurements. The TENACIOUS measurements will be taken at low altitudes which is uniquely different than IMAGE and TWINS, the two major future missions. From these low altitudes, high resolution images can be obtained that are not possible from high apogees–these allow a range of important scientific studies discussed below. In addition, the TENACIOUS data, when combined with these other contemporaneous data sets, will yield a meta-data set that is more powerful even than the sum of the individual components. Therefore, TENACIOUS is not only capable of highly self-contained scientific investigations, but will also contribute significantly to the other main NASA ENA missions presently being developed. Table reveals the complementarity of TENACIOUS to these other planned NASA missions (and the ongoing POLAR mission).

Science Implementation

We propose to achieve the scientific goals and objectives outlined above with optimized instrumentation on TENACIOUS. The instrumentation described below either has proven spaceflight heritage or is based, with low-or no-risk modifications, on hardware previously developed for NASA missions. The instrumentation includes an Imaging Energetic Particle Sensor, IEPS (for energetic protons, neutral atoms, and energetic electrons), and a pair of Tomographic Extreme-UltraViolet Spectrometers, TESS (for geocoronal imaging) each tuned either for daytime or nighttime observations. These instruments are described below; individual sensor specifications are summarized in accompanying tables.

Table 2. TENACIOUS ENA Imager Compared with Complementary Imagers

MISSION	TENACIOUS	IMAGE	TWINS	POLAR
Mission Type	UNEX	MIDEX	MOO	ISTP
Mission Cost (excluding launch)	<6 M$	∼45M$	∼15M$	>150M$
ENA Instrument	IEPS	HENA	MENA	IPS
Global Imaging	regional	yes	yes	yes
Energy Range (keV)	15–400	10–200	1 – 100	15-1500
Energy Resolution (ΔE/E)	0.15	0.7	0.4	0.15
Number of Energy Bins	8	4		16
Angular Resolution (°)	12 x 20	4 x 6	4 x 4	12 x 20
Typ. Projected Spatial Res.(Re)	0.03x0.05	0.5 x 0.75	0.5 x0.5	1.9 x 3.2
Typ. Temporal Res. (sec)	10	300	60	96
Typ. pixel dimension (mm)	2.0 x 3.5	1.5 x 1.5		1.5 x 3.0
Geom. Fact./pixel (cm^2-sr)	5x10^{-3}		1.4x10^{-3}	3x10^{-3}

Instrumentation

Imaging Energetic Particle Spectrometers (IEPS). The TENACIOUS Imaging Energetic Particle Spectrometers (IEPS) are designed to measure both pitch angle distributions of *in situ* protons and electrons as well as images of remotely-generated ENAs. The IEPS instrument (shown schematically in the left of Figure 5) is designed closely after the NASA POLAR/CEPPAD/IPS instrument (shown in its final flight configuration in the right of Figure 5). The IPS instrument is now returning very high quality measurements of both ions and ENAs from its POLAR orbit. The IEPS uses this well-proven design and has excellent flight heritage after over two full years of flawless operation. We note that not since the S3-3 satellite have there been comprehensive pitch angle measurements of this energy particle population (15 - 500 keV) at low altitudes.

In the IEPS, we propose to fly a near duplicate of the POLAR CEPPAD/IPS instrument. The investigators were central to the design, development, and fabrication of that instrument which is now delivering high quality neutral atom images from the POLAR orbit. The IEPS adopts the same technique of "pin-hole" particle imaging used in the POLAR instrument and which is described in detail in [*Blake et al.*(1995)]. The IEPS consists of a sensor head assembly with six identical sensor heads - three each for ions and neutrals. Unlike the IPS, a single head identical in form to those described below constitutes the electron sensor; it is not shown in Figure 5 for simplicity.

Each head uses pin-hole imaging to produce three 20-degree full-width-at-tenth-max pixels having a triangular response to an incident unidirectional beam. The pinhole optics defined by the entrance slit size, focal plane distance, and pixel location on the focal plane yield contiguous response curves that overlap at the tenth-max level. As a result, three non-overlapping 20-degree fields-of-view are obtained, yielding a 60-degree total polar field-of-view for each head. The three heads thus provide complete, non-overlapping 180-degree polar coverage segmented into nine, 20-degree pixels. All azimuthal (in the spin plane) angular responses are also triangular, with a full-width-at-tenth-max of 12 degree. The satellite spin thus sweeps out full 4π steradian coverage of the unit sphere on each 3-second rotation.

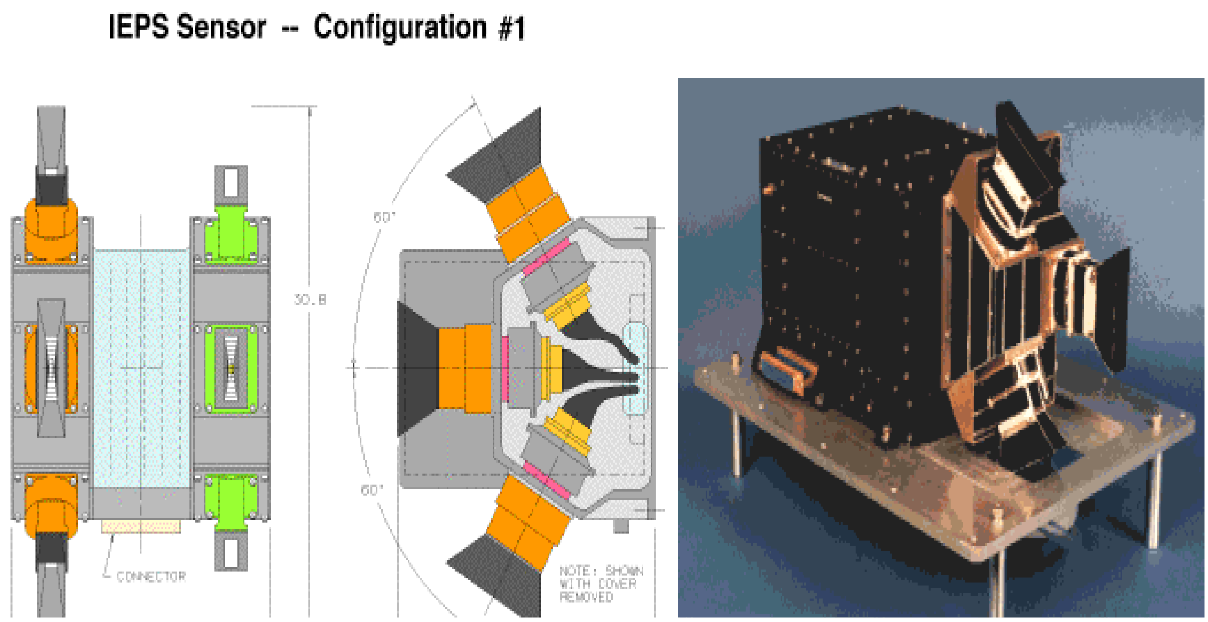

Figure 5. Engineering Drawing of IEPS and Photo of POLAR/CEPPAD/IPS

The IEPS, like the IPS, uses a segmented, monolithic solid state detector (SSD) at the focal plane of each pinhole camera. The SSD is run at full depletion with a nominal thickness of 150 mm. The pixels are defined on the detector through the process of ion implantation; each pixel is electrically decoupled from its neighbors by a guard ring structure. In the design and fabrication of these detectors, made by Micron Semiconductor, special care went into minimizing the dead layer on the implanted (entrance) side of the device. This special attention, along with low system electrical noise ($<$ 5 keV FWHM), has allowed us to establish a threshold for ion and neutral detection of $\sim$15 keV (although we note that the IPS has been run successfully on POLAR to as low as 12 keV). This low threshold is critical as it allows us to measure the substorm-related ENAs which have characteristic energies in the keV range rather than tens or hundreds of keV. As a consequence of the low energy threshold of the detectors, the ion/neutral telescopes are photosensitive to sun light and reflected "Earth-light." This responsivity to light is an important element for pointing requirements; the telescopes are oriented to minimize duration of direct Earth and Sun viewing. No sensor will sweep through the Sun's field-of-view, and in the worse case, some look directions may see the earth for as much as half a spin when it will be blinded. However, the recovery time of the detectors is short ($\sim$100 milliseconds) so that the important "up" directions for ENA detection will be free from light contamination.

Within the ion/neutral telescopes, a permanent magnet and baffle assembly eliminates to better than 99%, incident electrons with energies up to $\sim$1.5 MeV from the optical path, thereby providing a clean ion/neutral measurement. Sunshades and blackened collimators eliminate the scattered and Earth-reflected sunlight. Each $20^\circ \times 12^\circ$ IEPS pixel has a nominal CEPPAD-like geometrical factor of $\sim$ 5 x 10^{-3} cm^2-sr. During the concept study phase, simple modifications that could raise this value by a factor of two, with little mass penalty, will also be explored.

Within each sensor head, there is an independent detector board mount containing coupling capacitors and detector-biasing networks (typically 20V bias). Included also is circuitry for in-flight calibration with a charge pulser for each pixel and a field-effect transistor (FET) for each pixel. The outputs of this front-end analog signal are routed by mini-cables to the analog signal conditioning circuits via a pigtail. Each FET is coupled to standard charge sensitive preamplifiers that feed two stages of amplification, shaping, and baseline restoration. The shaping time is approximately 2.5 msec. The shaped signals are pulse-height analyzed on the digital preprocessor boards in a custom gate-array chip (KM-5) developed jointly with KMOS, Inc. for the POLAR mission. A stack of discriminators is built into the chip, allowing for up to 16 adjacent energy bins. The energy threshold and range of the analyzer can be adjusted by sending digital commands to digital-to-analog converters (DACs) internal to the chip. The chip can be run in one of two energy modes by selection of two independent resistor-divider chains in the chip: linear (ΔE constant) or logarithmic (ΔE/E = constant) bin spacing. The low- and high-energy reference voltage of each DAC can be controlled independently providing for a possible energy range of 0 to 1500 keV. Output logic pulses from individual bins are accumulated at high rate and then, for IEPS, are reduced in energy resolution to eight of the 16 possible bins. The data are accumulated in 24-bit scalers and read into memory at regular intervals, nominally 32 times per three-second spin. An in-flight calibration circuit is driven also from the digital board. It consists of two fixed precision amplitude pulses at 90 and 240 keV that drive the front-end electronics. A variable amplitude pulse generator, controlled via an 8 bit DAC, also provides calibration signals on command. A functional block diagram of the ion, neutral and electron sensors, and their analog and digital electronics is shown in Figure 6.

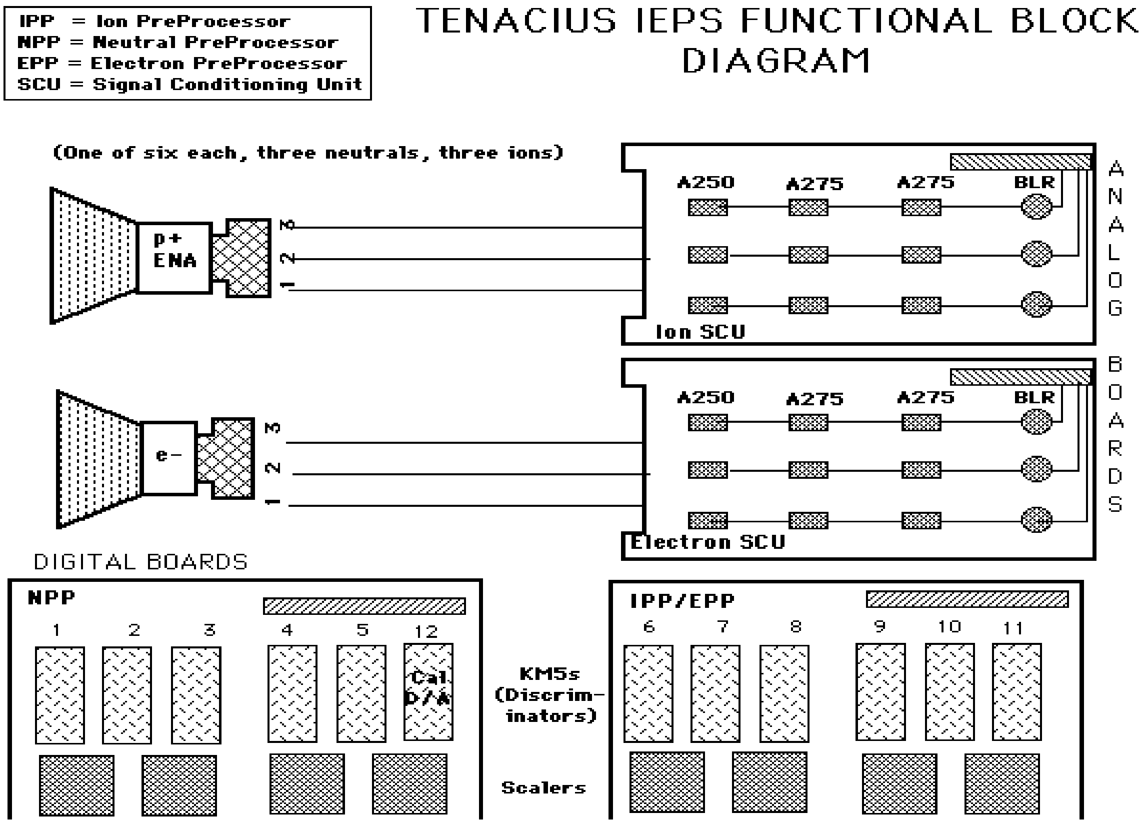

Figure 6. TENACIOUS IEPS functional block diagram.

Since we are sometimes in a charged particle foreground, it is important for us to know not only the ion population but also the electron population at similar energies. The IEPS includes also a single electron head, using the same effective design as the ion/neutral head. The electron detector is thicker and has a thick front contact that stops the incident ions and neutrals from detection, thus providing a clean electron measurement. The electron sensor will, like the ions/neutrals, have a commandable energy range but spanning now from 15 to $\sim$500 keV.

Compared to the POLAR instrument there is one principal difference in instrument design we propose and this will greatly enhance our ENA imaging. It is a value-added feature and if not fully implemented, will not in any manner compromise mission success. The extended design revolves around an inherent feature of the CEPPAD instrument. The POLAR/CEPPAD/IPS does not differentiate between ions and neutrals so it can only unambiguously identify the lower intensity neutrals when there is a negligible local energetic ion population (for example when it is near apogee, as in Figure 1).

At high polar altitudes, the spacecraft dwells for long periods in the magnetic lobes which are empty of energetic particles. At these times we can attribute particle fluxes coming from the direction of the magnetic equator to be energetic neutrals - a principal that both IMAGE and TWINS will rely on to varying degrees as well. Similarly, TENACIOUS IEPS will be making its principal measurements over the polar caps or beneath the radiation belts where neutrals are very well differentiated. Therefore, the prime instrument that only need work for mission success is the IPS component of the IEPS, which has already be shown to operate flawlessly for two years in orbit.

However, to add great value to our measurements, we wish to explore the way to extend our data accumulation into regions of foreground charged particle flux. At auroral and sub-auroral latitudes, TENACIOUS will encounter plasma sheet and ring current field lines where there exists both an ENA source but also a persistent flux of energetic ions. To allow for the unambiguous detection of energetic neutrals in the presence of this ion foreground, we shall modify the IPS design by including a redundant ion head (that is the reason for two sets of three heads) with an electrostatic ion rejection system similar to the one designed for the CLUSTER/RAPID/IIMS sensor [*Wilken et al.*(1997),]. The IIMS uses pre- and post-collimation with a multiple slit electrostatic deflection system using electric potentials of 10 kV. When the potential is off, the *in situ* ions pass through the optical path and are detected by the IEPS SSDs. When the retarding potentials are active, the electric fields reduce the transmission of ions with energies below 200 keV by three to four orders of magnitude [*Wilken et al.*(1997),]. By toggling the HV on and off, TENACIOUS IEPS will be able to alternatively view the local ion population and the line-of-sight integrated ENA emissions. Extension of the ENA measurements into the auroral region will be an exciting new prospect, but if not realized, will not impact our mission success criteria. Our science team has contacted the CLUSTER hardware team about providing expertise for the electrostatic shutter system; they have expressed interest in such a collaboration. We note that should either the ion or neutral head fail the other is a fully redundant backup capable of providing all the data needed for a successful mission.

Table 3. TENACIOUS IEPS Sensor Characteristics and System Resources

Sensor Characteristics	Neutrals	Protons	Electrons	Comments
Energy Range (keV)	15–400	15–400	15–400	8/16 log/lin channels
Field of View/pixel (deg)	12x20	12x20	12x20	Complete PA /spin = 3s
Number of polar pixels	9	9	3	No pixels include sun
Number of azimuthal sectors	32	32	8	
Temperature (Centigrade)	-40 to -5	-40 to -5	-40 to -5	Operating
	-40 to +35	-40 to +35	-40 to +35	Non-operating
Geometric factor/pixel ($cm^2 sr$)	0.005	0.05	0.001	
Geometric factor total ($cm^2 sr$)	0.05	0.05	0.01	
Total IEPS Resources				
Mass	8.9 kg			
Volume	$\sim$11,000 cm^3			
Power	10.5 W total; multiple regulated V: +/-5,28,4,7			
Telemetry	$\sim$3 kbps average, 2 contacts/day @ 160 Mbps/contact			
Processing	Microprocessor and memory to manipulate data and package telemetry			
Commanding	$<$8 kb/day of 16 bit commands, occasional memory uploads			

As noted above, the IEPS is largely based on the flight-proven NASA POLAR IPS instrument and has excellent heritage. The three POLAR/IPS sensor telescopes, mechanical housing, and analog and digital electronics have a measured combined mass of $\sim$3 kg. The IEPS is a second generation instrument based on the IPS and has already had some engineering development. It requires only minor modifications to advance from an "IPS" to an "IEPS". The estimated mass of three ion, three neutral, and one electron telescopes and supporting electronics and structure is $\sim$8.9 kg. The main IEPS volume is 308 x 190 x 189 mm. A baseline initial estimate of the IEPS resources and requirements, based on the configuration shown in Figure 5, are outlined in Table . This table includes the properties needed for the electrostatic deflector system noted above.

The properties above have been chosen not only to minimize changes from the IPS design, but also to meet our science requirements. These are driven largely by the possibility of doing tomography from the unique low-altitude environment.

The principle of tomography is really no different than the binocular vision most of us are born with. With one eye covered, we see only a flat image and must infer distance from size or overlapping images, but with both eyes open we are able to use parallax to judge distances much more precisely. In the same way, a slowly moving ENA imager, such as those on POLAR, IMAGE, or TWINS, sees a column integrated ENA map, and must infer the distance to the source from models of the emission region. Stereo images combined from multiple satellites helps greatly and that is the main thrust behind TWINS. However "depth" perception in stereoscopic vision is best when close to the source. We note, however, that TENACIOUS reduces the uncertainty by a whole new major step from mere stereoscopy. It takes advantage of its rapid, low-altitude orbit to effectively snap a parallax picture, every 3 seconds and thus every 21 kilometers along its orbital track.

If the ENA source is changing rapidly, such as is seen in POLAR ENA substorm studies, three seconds between exposures might blur the image. However, we do know from POLAR/IPS images that substorm ENA bursts, which have shorter timescales than storms, persist for 20 or more minutes, with the onset occurring over several minutes which is much slower than the exposure time. However, during that time, the spacecraft will have traversed the feet of the auroral field lines and imaged the evolution from widely varying angles. This is critical for unraveling the complex line-of-sight inversions necessary to back out the fundamental ion flux distributions. The optimal viewing geometries provided at low altitudes just simply cannot be accomplished by the slowly-moving, high-apogee satellites such as POLAR and other planned ENA missions.

A second requirement for tomography is that our data rate be sufficiently high to invert these exposures. We appeal to the aforementioned low-altitude instruments to predict a data rate for the IEPS ENA imager. At the POLAR/IPS perigee (4000 km altitude) we typically observe $\sim$4,000 counts/(sec -sr-cm^2-keV) with a threshold energy of $\sim$20 keV. The TIROS/MEPED instrument described in section D.1 is in a circular orbit at 850 km and it observes $\sim$1,000 counts/(sec-sr-cm2-keV) with its threshold energy of $\sim$30 keV. The ASTRID/PIPPI imager was in a circular orbit at $\sim$1000 km and recorded fluxes of 500-2000 counts/(sec-sr-cm2-keV) in an energy band of $\sim$26-37 keV. Note that the lower energy threshold of IPS more than compensates for its greater distance than TIROS from the assumed source. From these data, we can estimate a 10,000 counts/(sec-sr-cm2-keV) at the 15 keV threshold for TENACIOUS. If we divide the spin plane into 32 sectors, then we have $\sim$100 ms per sector with a 0.005 geometric factor resulting in about 5 counts per pixel, significantly above the expected cosmic ray noise of 0.1 counts/(sec-pixel) seen by IPS. At the lower average rates, summing of adjacent pixels may be required to improve counting statistics, but during moderate to large events, statistically significant images should be possible at our highest possible time resolution of $\sim$3 seconds. Part of the Phase A study will be devoted to finalizing the IEPS geometrical factors based on the most contemporary rates and trading that off against the mass and volume constraints. At this juncture, we are confident that excellent images can be made routinely even with the present POLAR-designed geometric factor.

To best resolve particle pitch angle distributions and neutral atom images, the instruments will be mounted such that the long axis of the instrument (vertical axis in Figure 5) points nominally along the spacecraft spin vector. That is precisely the orientation used on the POLAR spacecraft. To avoid the sun, the instrument will be rotated slightly away from the spin axis. In each spacecraft spin, the ion and neutral telescopes will map out the unit sphere. To maximize spatial coverage, the ion and neutral sensors may be mounted back-to-back as an alternative configuration to the one shown in Figure 5. The single electron telescope will be mounted perpendicular to the spin axis and will thus cover all pitch angles once per spin. Other telescope alignments that minimize resources and maximum science may be possible and will be studied in the Phase A period; we expect to proceed though with the baseline configuration just described.

The expected data rate for the IEPS sensor is approximately 3 kbps. This data is shared between the various instrument components and is commandable by uplinking a new telemetry table. The data are sampled at some high rate, stored in scalars, and then latched and moved into mass memory. The volume of the entire data set (21 look directions - 9 neutral, 9 ion, and 3 electron; each with eight energy bins; each sectored in nominally 32 sectors per spin) is far too large to fit our downlink limit. Therefore, we resample these data as we did on the POLAR/CEPPAD experiment; sampling the data into an 8-bit compressed format and undersampling those elements of the data cube that have fewer expected counts and allocating more telemetry to those parts of the data cube with more expected counts (i.e., at lower energies). For our calculations, we have used two ground contacts with TENACIOUS per day and a 160 Mbit download per contact.

Tomographic EUV Spectrographs (TESS). In order to infer neutral atmospheric species and tracer ion densities, needed to deconvolve the ENA emissions, we propose to fly two tomographic EUV spectrographs (TESS). This instrument has already been designed to fly on TERRIERS where it too will measure the same UV emissions. The TERRIERS design is perfectly suited to TENACIOUS. Atmospheric emis-sions of [O] (130.4nm), [He] (116.8 nm), and [H] (121.6nm) are targeted as well as is [O^+] (834nm). Additional important atmospheric emission lines are possible with the TESS instrument and will be prioritized during the Phase A study.

The TESS design offers the best compromise between spatial imaging, spectral resolution, and high sensitivity through the use of a novel spectrograph mount. The system consists of two basically identical spectrographs; one nightglow instrument, and one with a narrower slit to reduce sensitivity and increase spectral resolution for daytime operation. Figure 7 illustrates the optical design, which consists of only two optical elements: a slit assembly and a grating. These instruments are the same as those to be flown on TERRIERS with the same data and telemetry interfaces preserved for TENACIOUS.

We chose a Single Element Imaging Spectrograph (SEIS) [*Cotton et al.*(1994),], because its imaging capabilities and large FOV offer the highest possible throughput with high spatial resolution (0.4°) in a very small configuration (150 mm Roland circle). The sensitivity of the night TESS instrument is shown also in Figure 7. Furthermore, this design allowed us to vastly increase the science return by adding a nearly identical dayglow spectrograph for marginal cost.

Each TESS instrument will utilize a microchannel plate (MCP) detector with a wedge and strip readout. This type of detector has been flown many times including STP78-1, EUVE, UVX, DUVE, BEARS, CUBS and TERRIERS.

The requirements on the imaging detector were intentionally minimized in order to simplify the readout and data handling, lower the data rates and power consumption, and increase the reliability. To cover the pass bands at 1.0 nm resolution, only 256 bins are needed (2.5 bins/resel for the normal incidence spectrograph and 8 bins/resel for the grazing incidence spectrograph), and a 40 mm diameter active area. We expect a maximum (burst) count rate of 20 KHz for the entire bandpass (2.0-130.0 nm). This can be achieved with a microchannel plate (MCP) imaging, photon-counting detector with a wedge and strip readout. We chose this type of detector, because it offers very high signal-to-noise and the dynamic range that is necessary for the expected signal. Furthermore, the technology behind these detectors is very mature. We shall build the detector in house with our extensive experience with these types of detectors. The details of the operational characteristics of the wedge-and-strip readout are well known and life tests have been performed on MCP's in windowless EUV detectors, which show that they continue to operate nominally even after an exposure to 1013 counts/cm^2. This is more than adequate for the TENACIOUS mission with the expected count rates mentioned above. (At 20 kHz, the detector can operate continuously for 2.0 years.)

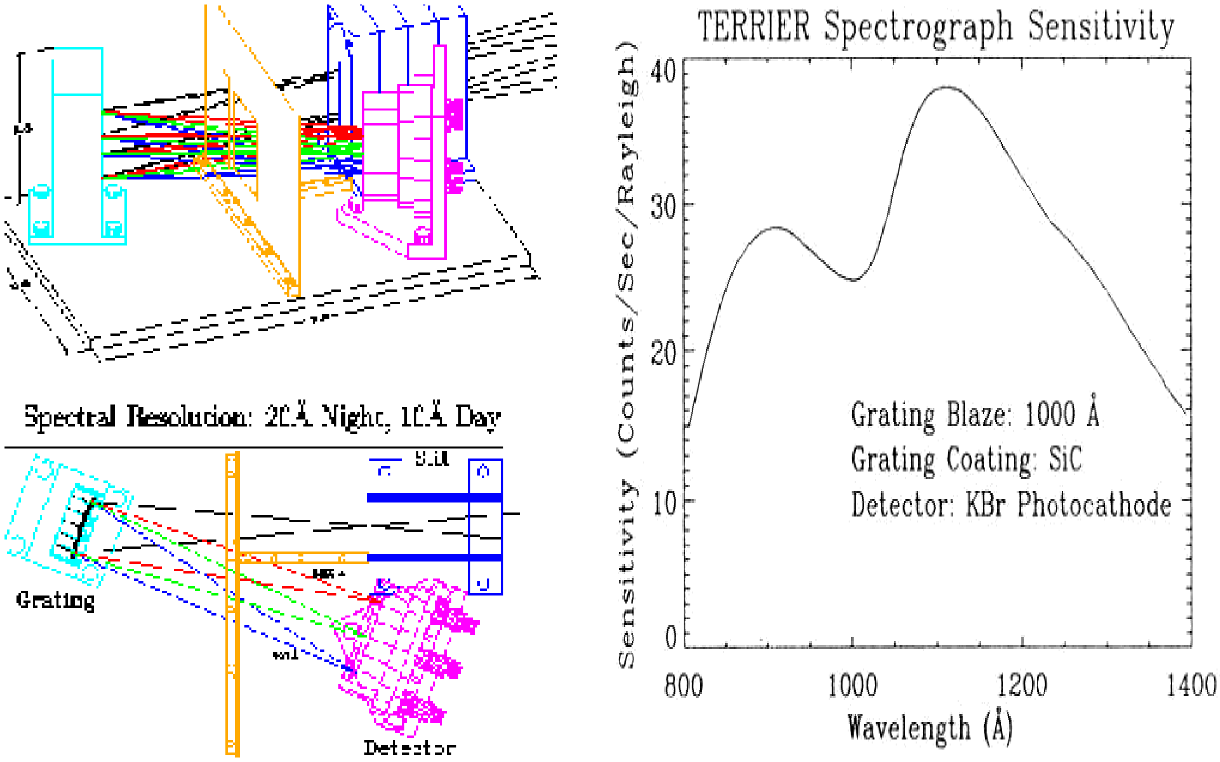

Figure 7. Optical Layout of TESS and Sensitivity of the Nightside TESS Instrument

The TESS detector bodies will be constructed of brazed ceramic/metal for ruggedness, simplicity and reliability. This type of construction has been used for the detectors in the ALEXIS satellite, identical to the TERRIERS satellite and in rocket experiments. These programs have demonstrated that the type of design scheme proposed is compatible with space-flight requirements (vibration, thermal, etc.) The microchannel plates will be held in place by an annular spring ring applying an even pressure around the circumference of the MCP stack. A stack of three back to back MCP's is baselined, each having a channel diameter of 12.55 mm, and a channel length to diameter ratio of 80:1. This MCP configuration has been used in 23 spacecraft, 1 shuttle, and 11 rocket experiments, and gives high gain (>2x10^7) with tight pulse height distributions (<50% FWHM) and low background rates (<0.5 events/s-cm^2).

We intend to deposit a KBr photocathode on the MCPs to enhance the quantum efficiency between 80.0-140.0 nm (about 20%). The two options in this region are KBr and CsI. We chose KBr since it offers better stability and a little higher quantum efficiency.

The wedge and strip position readout anode will be mounted on the signal feedthroughs about 1 cm behind the MCP stack. An appropriate design is the three-element anode which has been used extensively for other space missions. The detector will not be the dominating term in either of the spectrographs resolution budgets. The required resolution performance (90 nm) may be obtained with a standard wedge and strip design. The predicted resolution for a 35 mm diameter wedge and strip pattern on a quartz substrate is 50 nm. We have assumed input referred noise levels of 1000 e- rms for the wedge and strip, and 1500 e- rms for the zigzag. The latter noise levels are modest for charge sensitive preamplifiers when loaded with the $<$200 pF capacitance of this anode design.

We propose to calibrate the detector in flight by periodically taking dayglow spectra. Using the known lines (e.g. 83.4, 98.9, 130.4, 135.6 nm), we can detect and correct for changes in the electronics linearity, gain and DC offsets to the optical resolution of the spectrographs.

Conclusion: Technical Issues and Advantages of TENACIOUS (LEO Orbit) for Magnetospheric Imagers

The instruments outlined above to carry out the mission goals all have excellent flight heritage. In some cases, the proposed instrument will need only modest modifications from a present design or combination of designs. Furthermore, the TENACIOUS science team has excellent experience with the design, development, delivery, operation, and analysis of the data from these types of sensors.

We note that low Earth orbit is a novel, and in many ways an optimal, location to perform magnetospheric neutral atom imaging. We have noted the advantages previously. One concern is the multiple scattering of ENAs that can occur in the denser regions of the atmosphere. This question has been treated theoretically and shown that altitudes above 850 kilometers are nearly scatter-free. Altitudes at 1000 kilometers or higher are optimal from an ENA point of view, but higher altitudes introduce radiation damage effects to sensor electronics. [*Soraas and Aarsnes*(1996)] showed from their rocket data that even at 450 kilometers the effects of scattering were still surprisingly minimal. Indeed, [*Gruntman*(1997)] alluded to the fact that problems attributed to multiple scattering have probably been overestimated based on simple theory. Therefore we are targeting an apogee altitude of TENACIOUS at 1000 km to be into a single encounter (optically thin) ENA regime. Anything above 850 km would be acceptable so we are actually very insensitive to exact altitude. Our insertion altitude is $\sim$ 470 kilometers, so even in the worst case, the good science achieved by the rocket flight gives us excellent confidence for mission success.

The initial orbital insertion will place TENACIOUS into a 10:30-22:30 UT sun-synchronous plane. During our motor burn to raise apogee, some of the Dv will go into a change in inclination. We estimate that an approximately four-degree plane angle change is possible with residual fuel beyond that for the 1000 km apogee raise maneuver. This change in sun-synchronicity will allow the orbit plane to slowly evolve with time at about 0.5 degrees/day. Therefore, we will cover all local times in one year and come back to the same configuration (with the same ascending node) in two years. This situation is desirable as it allows us to measure low-altitude ENAs at all local times. At the same time, we are almost totally insensitive to the rate of orbital motion; mission success is very weakly dependent on it. We will focus initially on substorm ENAs as the 22:30 UT local time sector has been observed by POLAR to be the most probable location for ENA generation at substorm onset. As we move through other local time sectors throughout the two-year mission lifetime, different physics as appropriate will be emphasized.

References

Alothman, M. J. and T. A. Fritz. Investigation of cusp energetic particle events signature in the high latitude trapping boundary. *EOS Trans. Suppl.*, *79*(17), S297, 1998.

Barabash, S., P. C:son Brandt, O. Norberg, R. Lundin, E. C. Roelof, C. J. Chase, B. H. Mauk, and H. Koskinnen. Energetic neutral atom imaging by the ASTRID microsatellite. *Adv. Space Res.*, 1997.

Blake, J. B. et al. CEPPAD: Comprehensive energetic particle and pitch angle distribution experiment on POLAR. In C. T. Russell, editor, *The Global Geospace Mission*, pages 531–562. Kluwer Academic Publishers, 1995.

Brandt, P. C:Son, S. Barabash, O. Norberg, R. Lundin, E. C. Roelof, C. J. Chase, B. H. Mauk, and M. Thomsen. Ena imaging from the Swedish microsatellite ASTRID during the magnetic storm of 8 February 1995. *Adv. Space Res.*, 1999.

Cotton, D. M., T. Cook, and S. Chakrabarti. A single element imaging spectrograph. *Applied Optics*, *33*, 1994.

Gruntman, M. Energetic neutral atom imaging of space plasmas. *Rev. Sci. Inst.*, *68*, 3617–3656, 1997.

Henderson, M., G. Reeves, A. Jorgenson, H. Spence, R. Sheldon, B. Blake, and J. Fennell. First energetic neutral atom images from POLAR/CEPPAD/IPS. *Geophys. Res. Lett.*, *24*, 1167–1170, 1997.

Jorgensen, A. M., H. E. Spence, M. G. Henderson, G. D. Reeves, M. Sugiura, and T. Kamei. Global energetic neutral atom (ENA) measurements and their associeation with the Dst index. *Geophys. Res. Lett.*, *24*, 1167–1170, 1997.

Lui, A. T. Y., D. J. Williams, E. C. Roelof, R. W. McEntire, and D. G. Mitchell. First composition measurements of energetic neutral atoms. *Geophys. Res. Lett.*, *23*, 2641–2644, 1996.

Milillo, A., S. Orsini, I. A. Daglis, and G. Bellucci. Low-altitude energetic neutral atoms imaging of the inner magnetosphere: A geometrical method to identify the energetic neutral atoms contributions from different magnetospheric regions. *J. Geophys. Res.*, *101*, 27123, 1996.

Orsini, S., I. A. Daglis, M. Candidi, K. Hsieh, S. Livi, and B. Wilken. Model calculation of energetic neutral atoms precipitation at low altitudes. *J. Geophys. Res.*, *99*, 13489, 1994.

Roelof, E. C., D. G. Mitchell, and D. J. Williams. Energetic neutral atoms (E$\sim$50keV from the ring current: IMPS 7/8 and ISEE 1. *J. Geophys. Res.*, *90*, 10991, 1985.

Roelof, E. C. Energetic neutral atom image of a storm-time ring current. *Geophys. Res. Lett.*, *14*, 652–655, 1987.

Roelof, E. C. ENA emission from nearly mirroring magnetospheric ions interacting with the exosphere. *Adv. Space Res.*, *20*, 361, 1997a.

Roelof, E. C. Energetic neutral atom imaging of magnetospheric ions from high and low altitude spacecraft. *Adv. Space Res.*, *20*, 341, 1997b.

Sheldon, R. B. and D. C. Hamilton. Ion transport and loss in the earth's quiet ring current 1. data and standard model. *J. Geophys. Res.*, *98*, 13,491–13,508, 1993.

Sheldon, R. B. and H. E. Spence. A new magnetic storm model. In J. Horwitz, editor, *Geospace Mass and Energy Flow: Results from the International Solar-Terrestrial Physics Program*, pages 349–354, Washington, D.C., 1998. AGU.

Sheldon, R. B., H. E. Spence, and J. F. Fennell. Observation of 40 kev field-aligned ion beams. *Geophys. Res. Lett.*, *25*, 1617–1620, 1998.

Soraas, F. and K. Aarsnes. Observations of ENA in and near a proton arc. *Geophys. Res. Lett.*, *23*, 2959–2962, 1996.

Spence, H. E., A. M. Jorgensen, T. A. Fritz, R. B. Sheldon, M. G. Henderson, G. D. Reeves, J. B. Blake, J. F. Fennell, and D. N. Baker. The substorm injection revealed: global ENA images and simultaneous multipoint observations of the substorm lifecycle. *EOS Trans. Suppl.*, page F612, 1997.

Wilken, B. et al. RAPID: the imaging energetic particle spectrometer on CLUSTER. *Space Sci. Rev.*, *79*, 399, 1997.

UAH Physics Dept OB201, Huntsville AL 35899

This preprint was prepared with AGU's LaTeX macros v4. File jatp1 formatted July 21, 1999.